AIP | The Journal of Chemical Physics

Absolute Differential Cross Sections of Elastically Scattered Electrons. I. He, N2, and CO at 500 eV

J. Philip Bromberg

Citation: J. Chem. Phys. **50**, 3906 (1969); doi: 10.1063/1.1671647
View online: http://dx.doi.org/10.1063/1.1671647
View Table of Contents: http://jcp.aip.org/resource/1/JCPSA6/v50/i9
Published by the American Institute of Physics.

Absolute Differential Cross Sections of Elastically Scattered Electrons. I. He, N_2, and CO at 500 eV*

J. PHILIP BROMBERG
Mellon Institute and the Department of Chemistry, Carnegie-Mellon University, 4400 Fifth Avenue, Pittsburgh, Pennsylvania 15213

(Received 7 May 1968)

An electron spectrometer especially designed for the study of elastic scattering has been constructed and used to measure absolute differential elastic cross sections of 500-eV electrons scattered from He, CO, and N_2. Comparison with calculated values for He indicates that the first Born approximation with exchange gives results which agree with experiment to within 2% at angles greater than 18°. At small angles the observed cross sections exceed the calculated by a large factor. The cross sections for N_2 and CO change with angle in very similar ways.

I. INTRODUCTION

This work forms part of a continuing study of inelastic collision cross sections being carried out at this laboratory. Both here and elsewhere, inelastic cross sections are usually reported on a relative basis; when absolute measurements are reported, they have usually been made absolute by comparison with a theoretically calculated cross section, for example, that of the $1\,^1S \rightarrow 2\,^1P$ transition for He.[1] This work was undertaken to provide a convenient experimental basis for the determination of absolute inelastic collision cross sections by providing an absolutely determined peak on an electron-impact spectra well separated from the inelastic peaks.

The usual end product in a scattering experiment is a spectrum relating the number of scattered electrons to the energy lost in the collision. If the absolute scattering cross section of any single peak is known, then all the transitions may be converted to absolute cross sections by comparison with the known peak. Thus, for absolute measurements it will suffice to determine any arbitrary peak absolutely, and infer the rest from that one. The most suitable peak for calibration purposes will be one which is both intense, and easily resolvable; that peak is the elastic transition peak, which is separated by many electron volts from the first inelastic transition. We thus measure absolute elastic collision cross sections to serve as a calibration standard for inelastic collision cross sections.

The precision of the instrument was extensively checked in a series of measurements at 500 eV with N_2, CO, and He chosen for their interest here and in other laboratories. This paper contains a complete description of our apparatus and methodology. It is planned to extend these measurements to lower electron energies, and perhaps to include a number of other gases. These data will be published as they become available, though in much abbreviated form.

* Supported in part by the U.S. Air Force Office of Scientific Research under Grant AF-AFOSR-61-63; Contract AF 49(638)-1668; Grant AFOSR 68-1495.

[1] E. N. Lassettre and E. A. Jones, J. Chem. Phys. **40**, 1218 (1964).

II. EXPERIMENTAL

The measurement of collision cross sections on an absolute basis imposes many conditions on the measuring apparatus which must be met if the measured cross sections are to be reliable. In this section we first describe these general conditions, followed by a description of the various parts of our apparatus and how these conditions have been met; finally we shall present our experimentally measured cross sections, including a discussion of the errors.

General Considerations

Electrons are generated in the electron gun, and enter the collision chamber in the form of a well collimated beam of known energy and of small energy spread. A primary beam detector, shown in Fig. 1 as a dashed box directly ahead of the electron gun exit, must be removable through the walls of the vacuum chamber and replaceable to a precisely determined position. S-1 and S-2 are two slits, or pinholes, or combination thereof, of precisely determined sizes. They must be accurately aligned and positioned relative to each other and also to the primary beam so that ϕ, the wedge angle, and hence l, the length of the scattering volume may be accurately determined. The scattered beam detector must detect all electrons which have been elastically scattered into solid angle Ω at angle θ, and must have sufficient resolution to reject all other electrons, i.e., inelastically scattered electrons, secondaries, and ions. The angle θ is changed by rotating either the gun or detector. The primary electron beam path and the line of centers of S-1 and S-2 form a plane which must be kept constant during rotation.

A dynamical situation exists in the collision chamber in which gas is slowly leaked in through the inlet, and pumped out through slits and other channels connecting the collision chamber with the lower pressure side of the system. A large-sized chamber will allow each gas molecule to undergo a large number of collisions before being pumped out, thereby ensuring pressure equilibration. An absolute pressure gauge must, of course, be provided.

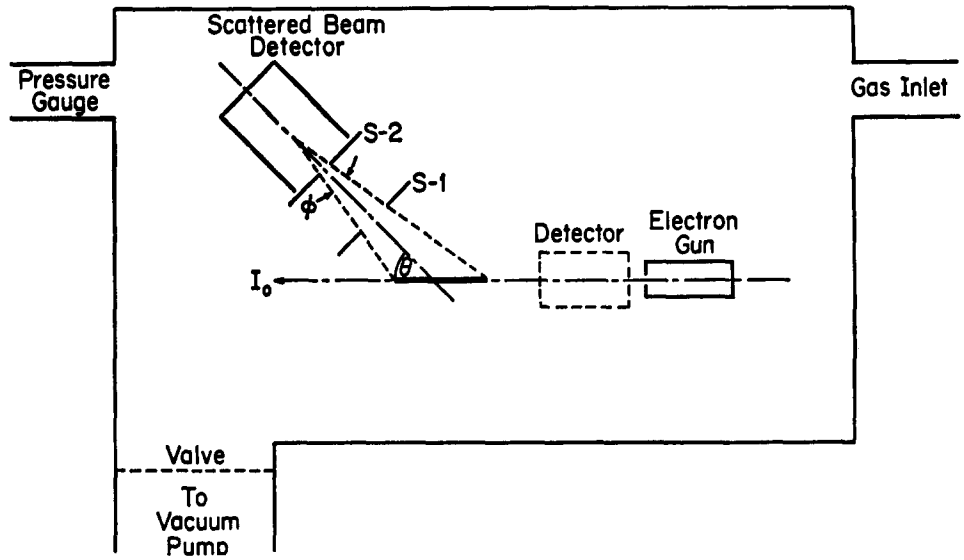

FIG. 1. General schematic spectrometer.

Apparatus

Vacuum System

Figure 2 shows a cross-sectional view of the spectrometer designed to satisfy the hitherto mentioned criteria. (Numbers appearing in the text in parentheses refer to part numbers in Fig. 2.) The section is that of a plane perpendicular to the plane of rotation through the electron beam path with the velocity analyzer set at 0°. Except for slits, bearings, electrical connections, and insulators the entire assembly was constructed of type 304 stainless steel; only metals or ceramic materials were in contact with the vacuum. All welds were by the heliarc process and found to be leak-free using a helium leak detector. The outer jacket was a 17-in.-o.d., $\frac{1}{8}$-in. wall thickness stainless steel tube. The removable top flange (1) was gasketed with two concentric silverplated stainless steel O-rings, the space between the two rings being pumped by a small mechanical pump. A 300-liter/sec ion pump connected to the lower flange (2) was capable of pumping the entire system to below 10^{-9} torr under favorable conditions.

The system may be conveniently subdivided into four regions: collision chamber (I); electron gun chamber (II); analyzer chamber (III); and bottom chamber (IV). The last three chambers together form the high-vacuum region of the instrument. Two stainless steel Swagelok fittings were welded to opposite sides of the collision chamber walls for gas inlet, and McLeod gauge access. In actual operation with N_2 and CO a pressure differential of 1000-fold was maintained between the collision chamber and the ion pump as measured by McLeod gauge and ion pump meter. The major sources of leakage between the two regions are the pinholes to gun and analyzer chambers, and the region between the analyzer housing shaft (3) and the baseplate (4). All other leaks are presumed insignificant in comparison. The volume of the collision chamber is about 30 liters. For N_2 at a pressure of 10^{-3} torr the estimated pumping rate from the collision chamber is 0.3 liters/sec, giving each molecule a life of about 100 sec in the collision chamber. Each molecule undergoes 10^6 collisions in this time; we thus assume a pressure equilibrium in the collision chamber.

The collision chamber is pumped to ultimate vacuum by opening the inner valve (5). This is accomplished by adjusting the bellows sealed linear feedthrough[2] attached to the flange (7). In the closed position the valve is pressed against the lower plate by a spring. The roughing system consists of a small 2-in. air-cooled NRC diffusion pump backed by a small mechanical pump. Unfortunately, the ion pump was incapable of pumping helium at the required pressures; all runs on helium were made with the ion pump shut off, pumping being achieved with the roughing system, which was capable of a pressure below 10^{-7} torr. Scattering gases were introduced through a Granville–Phillips variable leak; pressures were measured with a McLeod gauge, to be described later. A magnetic shield surrounded the apparatus to reduce the effects of the earth's and ion pump's magnetic fields.

Primary Beam System

The electron gun consisting of four gold-plated copper electrodes and an oxide-coated cathode (23) was held snugly in the gun retaining ring (8). The geometrical configuration of the electrodes and cathode is identical to that in the gun described elsewhere.[3] The

[2] We found that the replaceable bellows section for the Ultek $1\frac{1}{2}$-in. bellows sealed stainless-steel valve served as an excellent linear feedthrough.

[3] A. M. Skerbele and E. N. Lassettre, J. Chem. Phys. **40**, 1271 (1964).

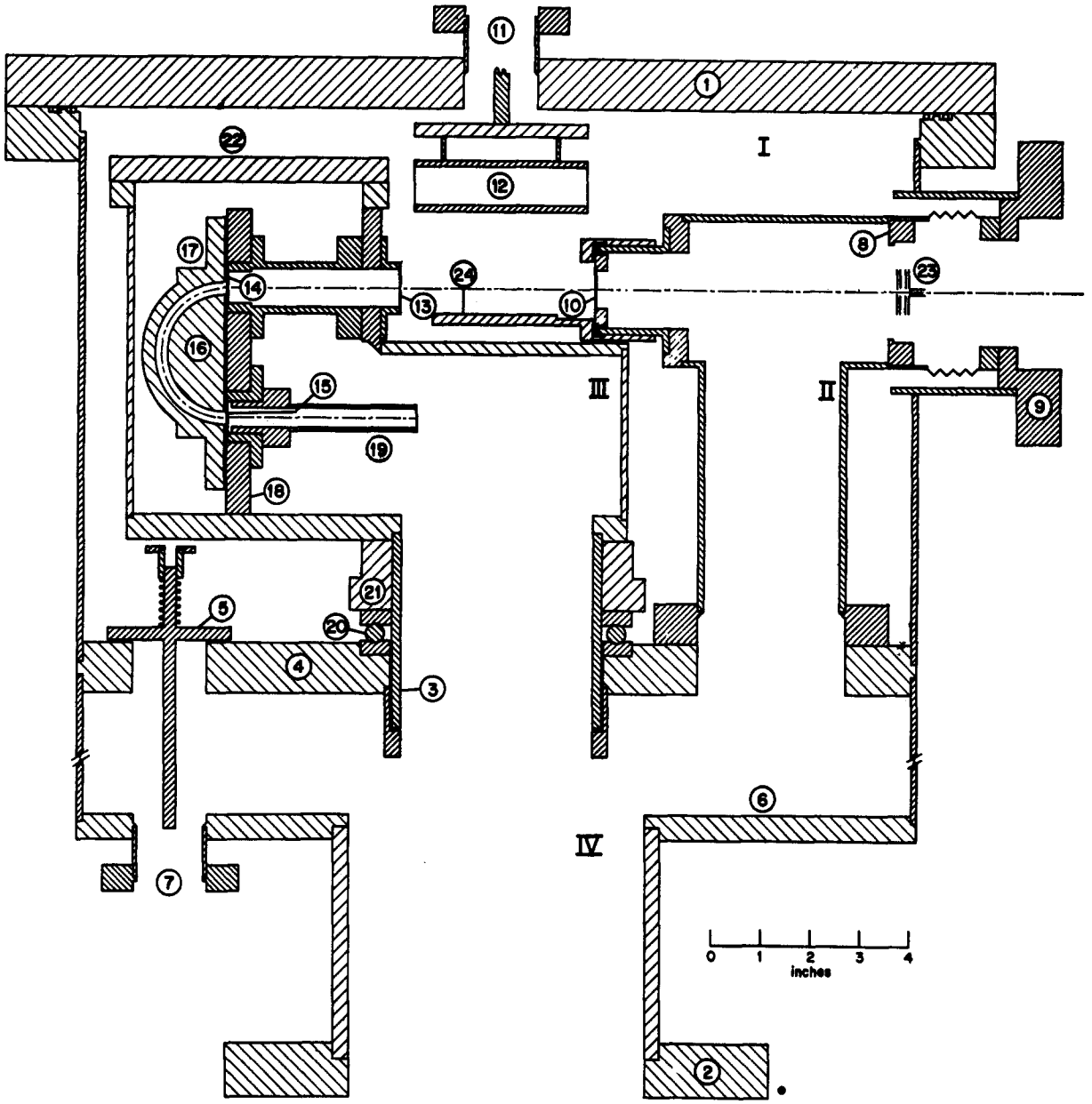

FIG. 2. Apparatus for absolute-cross-section measurements.

exit pinhole from the gun was 1 mm in diameter. To ensure a well-collimated beam an additional 1.00-mm-diam pinhole (10) was placed 15 cm downstream from the electron gun; this pinhole was connected to ground through a microammeter.

Primary beam current, I_0, was measured by a shielded Faraday cylinder (12) which was raised and lowered by a linear feedthrough in flange (11). The cylinder was accurately positioned by seating it in a cut-away cylinder (24) securely fastened to the gun chamber and concentric with the electron beam path. The current from the cylinder passed to ground through a 1000-Ω precision resistor, and was determined by measuring the voltage drop across the resistor with a Leeds and Northrup microvolt amplifier. A 30-MΩ resistor was placed in series with the standard resistor to keep the cylinder sufficiently below ground to reject secondary electrons. The entrance to the cylinder was a 4-mm-diam pinhole; the length was 64 mm giving a length to entrance ratio of 15:1. To test for the presence of secondaries the operating voltage of the cylinder was varied during an actual measurement. I_0 was found to be independent of voltage over a range of some 200 V. Primary beam currents ranged between 1 and 2 μA

TABLE I. Slit parameters.

	Slit system I	Slit system II	Slit system III
s=width of slit S-1 (mm)[a]	0.938	1.170	1.817
	0.950	1.180	1.811
	0.944	1.171	1.807
	0.944±0.006	1.174±0.005	1.812±0.005
p=diam of pinhole S-2 (mm)[a]	0.211_3	0.307_8	0.639_7
	0.214_1	0.310_0	0.640_6
	0.213_1	0.310_7	0.642_7
	0.212_8±0.003	0.309_5±0.003	0.641_0±0.003
Diameter of pinhole S-3 (mm)	0.564	0.641	0.983
		(0.983)[b]	
d=distance between S-1 and S-2 (mm)	90.55	90.55	90.55
d'=distance from S-1 to rotation axis (mm)	49.02	49.02	49.02
wedge angle $\phi \sim \tan\phi = s/d$ (rad)	0.01043	0.01297	0.02001
L=length of scattering volume at 90° angle=$(d+d')s/d$ (mm)	1.4550	1.8096	2.7929
Ω=solid angle subtended by S-2 about rotation axis (sterad)	1.826×10^{-6}	3.862×10^{-6}	16.566×10^{-6}

[a] The first number was obtained with the micrometer eyepiece, the second with the Gaertner microscope, and the third from the areas of photomicrographs. The fourth number is the average of the first three.

[b] Two different exit pinholes were used to check the transmission of this slit system. The system using the 0.938-mm exit pinhole will be referred to as system II′.

depending on the condition of the emitter and the pressure in the chamber. The current to slit (10) ranged between 40 and 90 μA.

Slit Systems

Slits S-1 (13) and S-2 (14) determine a wedge of angle ϕ which intersects the beam I_0. The relevant dimensions of the slit systems are listed in Table I. Three different slit systems were used in this work. S-1 is a narrow slit of length 1 cm; S-2 and S-3 (15) are small pinholes. Three independent measurements were made of each critical slit and pinhole. First they were measured on a Zeiss metallurgical microscope using a filar micrometer eyepiece. The widths of slits S-1 were measured at intervals of 1 mm and averaged over the central 5 mm. Diameters of pinholes S-2 were measured at four positions rotating the piece by 45° between measurements; each piece was measured at three different magnifications, the eyepiece being calibrated against a stage micrometer at each magnification. The out of roundness of the holes was less than 1% in all cases as indicated by the variation of diameters. Second, these measurements were repeated using a Gaertner toolmakers microscope fitted with a high power objective, the dimensions being obtained directly from the calibrated screw. In this case, the slitwidths were measured at intervals of 0.2 mm and averaged over the central 2 mm. Finally, photomicrographs of the slits and pinholes were taken, and the relevant dimensions determined from the areas as measured by a planimeter. The scale was provided by photomicrographs of the stage micrometer taken immediately afterward with all settings unchanged. Figure 3 shows photographs of the pinholes.

The three measurements are listed in Table I. The dimensions were taken as the average of the three determinations. The total spread in the measurements was of the order of 1% or less for the six dimensions. The uncertainty in each dimension was taken as the larger of 0.003 mm and the average deviation in the three determinations. The fractional error in the term $(I\Omega)$ in Eq. (1) is given by $2\delta_p+\delta_s$ where δ_p and δ_s are the fractional uncertainties for pinholes and slits, re-

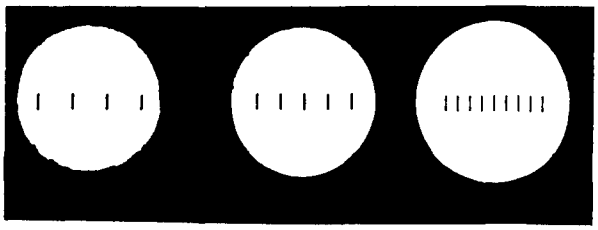

FIG. 3. Photomicrographs of analyzer entrance pinholes; scale lines are 0.0500 mm apart.

spectively. The fractional errors due to slit measurements are 0.0345, 0.0236, and 0.0121 for slit systems I, II, and III, respectively. They are very nearly in the ratio of 3:2:1; thus their weights in least-squared calculations will be 1, 4, and 9. The total fractional uncertainty in $\sigma(\theta)$ due to errors in slit and pinhole dimensions will then be 0.0103.

The absolute scattering cross section is given by

$$\sigma(\theta)=I/PnI_0\Omega l, \tag{1}$$

where I is the electron current scattered into the solid angle Ω at scattering angle θ; P is the pressure in the scattering chamber in millitorricelli; n is the number of molecules per unit length of scattering volume at 1 mtorr (assuming a temperature of 296°K, and a 1-mm diam of the incident electron beam, $n=2.5628\times10^{10}$ molecules $\text{mtorr}^{-1}\cdot\text{mm}^{-1}$. It should be noted that the cross-sectional area term in n is exactly canceled by the cross-sectional area term in I_0; hence the exact diameter of the exit pinhole is unimportant); Ω is the solid angle subtended by S-2 about the rotation axis; l is the length of the scattering volume; and I_0 is the incident beam current density.

In actual fact, Ω is not constant over the entire length of the scattering volume, and the correct value for the product term Ωl in Eq. (1) must be obtained by integration over the entire scattering length. It has been demonstrated[4] that at scattering angle θ this term may be replaced by

$$(\Omega l)\,(\text{effective})=\pi p^2L/4(d+d')^2\sin\theta, \tag{2}$$

where the quantities are as defined in Table I. In our experimental arrangement, the pinholes are sufficiently small, and the distance $(d+d')$ sufficiently large that second-order corrections to Eq. (2) are negligible even at the smallest angles used.

Scattered Beam Detector

The velocity analyzer consists of two concentric hemispheres, parts (16) and (17) on Fig. 2. The hemispheres were accurately located on the analyzer baseplate (18) with 0.1250-in.-diam sapphire ball bearings fitting into countersunk holes in hemispheres and baseplate; the holes were countersunk to allow a clearance of 0.020 in. between hemispheres and baseplate. The assembly was held rigid with insulated screws. The operation of the hemispherical analyzer was first described by Purcell.[5]

The hemispherical analyzer focuses an image of the entrance pinhole, S-2, on the exit pinhole, S-3, the condition for focus being

$$V_f=E[(R_0/R_i)-(R_i/R_0)], \tag{3}$$

where V_f is the focusing potential between the two hemispheres for electrons traveling through the analyzer with kinetic energy E; R_0 and R_i are the radii of outer and inner hemispheres. For our analyzer, $R_0=$ 1.406 in., $R_i=1.156$ in., and the mean radius, $R_m=$ 1.281 in.; thus $V_f=0.3941E$. The resolution of the analyzer as a fraction of the kinetic energy of the electrons passing through the analyzer is given by $\Delta E/E=p/2R_m=0.0154p$ where p is the slit size in millimeters.

Figure 4 shows an incident electron beam I_0 impinging on S-2, which we take to be infinitesimally small. If the incident beam has a spread in energy, δE, then the analyzer will spread the beam such that a finite image of diameter $2Y$ is formed on the exit pinhole, S-3. If the transmission of the analyzer is to be unity, then the diameter of pinhole S-3 must be at least as large as $2Y$. For finite S-2, the diameter of S-3 must exceed the diameter of S-2 by at least $2Y$ to ensure that all electrons of interest which enter S-2 will exit at S-3. From Purcell's paper, $Y=R_m\delta E/E$, where E is the kinetic energy of the electrons during their passage through the analyzer.

Electrons are generated at the cathode at -500.00 V and pass through grounded pinholes before entering the grounded collision chamber. Thus they approach S-2 with an energy of 500 eV, and pass through the analyzer with an energy determined by the potential at R_m. In the usual mode of operation the inner hemisphere is grounded and the outer run at a potential V_0 below ground; for 500-eV electrons V_0 is -157 V and the electrons pass through the analyzer with an energy of 398 eV. Under these conditions, assuming an energy spread of 0.5 eV in the primary beam, $Y=0.08$ mm. In all slit systems used, the diameter of S-3 exceeded the diameter of S-2 by at least 0.33 mm. That all electrons of interest entering at S-2 do, in fact, leave S-3 was experimentally verified by two independent techniques.

First, by operating the inner hemisphere above ground we may increase the energy of the electrons as they pass through the analyzer; conversely, their energy may be further decreased by operating the inner hemisphere below ground. Since the energy spread δE is fixed at the cathode, increasing their speed through the analyzer will decrease Y in Fig. 4. Thus the transmission coefficient may be checked by varying the speed at

[4] C. L. Critchfield and D. C. Dodder, Phys. Rev. **75**, 419 (1949); C. E. Kuyatt, *Methods of Experimental Physics* (Academic Press Inc., New York, 1968), Vol. 7A.

[5] E. M. Purcell, Phys. Rev. **54**, 818 (1938).

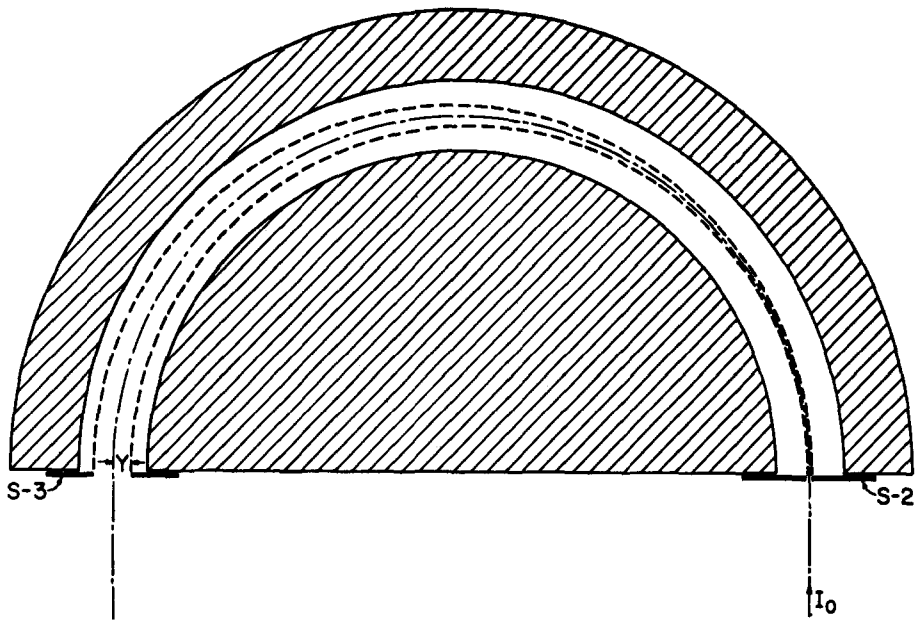

FIG. 4. Electron path through the analyzer showing the divergence caused by the energy spread in the incident beam.

which electrons pass through the analyzer while maintaining a constant I_0. Figure 5 shows the results of such a test using slit system III. Here the potential of the inner hemisphere is fixed at the value required for the indicated energies, while the potential of the outer hemisphere was slowly varied with a synchronous motor, the current through S-3 being displayed on a recorder; I_0 was a 1.00-μA beam of 500-eV electrons. It is seen that the beam passing through S-3 increased in intensity from 100 to 300 eV; between 300 and 700 eV the beam intensity was constant indicating that the transmission coefficient is, indeed, unity if the electrons travel through the analyzer with energies greater than 300 eV. The peak at 398 eV was taken with the inner hemisphere grounded, which is the usual mode of operation. An interesting feature of Fig. 5 is the fact that the curves at 300 eV or greater all have flat tops. This is a criterion for establishing that the transmission coefficient is unity, as it indicates that there is a spread in voltage at which all electrons pass through S-3; for less than unit transmission the peak is curved as seen in the 100- and 200-eV curves. This feature greatly simplifies current measurements; the potential of the outer hemisphere is adjusted to correspond with the center of the flat peak, and the current passing through S-3 measured. The system is thus deliberately operated under conditions of poor resolution, but not so poor that the inelastic peak is not separated from the elastic. Figure 6 shows a set of CO spectra for 500-eV electrons at 2° under different analyzer conditions. The resolution is such that the peaks are just barely separated at the smallest angle under normal conditions.

Second, and more critically, a set of scattering measurements was made on He using slit system II with pinhole diameters of 0.310 and 0.641 mm for entrance and exit slits, respectively. The exit pinhole was then replaced by a 0.983-mm-diam pinhole and two additional sets of points taken at all angles with this new slit system II′. If the transmission of the analyzer were less than unity for system II, then the measurements with II′ would yield larger scattering cross sections. The data for both systems are plotted in Fig. 8; there is no significant difference between the results for the two systems, the data for both falling on the same straight line. We feel that this convincingly demonstrates that the transmission coefficient is unity, that the analyzers were constructed with sufficient tolerances, and that the fringing fields which exist at the entrance and exit to the analyzer are sufficiently small that they do not affect our measurements.

A Faraday cylinder was placed directly behind S-3 contained in shield (19); the cylinder was insulated from and positioned in the shield with precision-drilled sapphire insulators. The entrance hole and length of this cylinder are identical to those of the primary beam Faraday cylinder; thus any inefficiency in collection ability will manifest itself equally in the two cylinders leaving the ratio I/I_0 unaffected. It was found that varying the cylinder voltage from -0.3 to -30 V had no effect on the measured current, and we assume the absence of secondary electrons and ions. The current to the Faraday cylinder was read with a Cary vibrating-reed electrometer by measuring the voltage drop to ground across precision high resistors built into the instrument. The output from the electrometer was fed to a recorder, and the current read from that. The calibration of the meters and recorders was checked with suitable voltage standards. The calibration of the resistors is described in the appendix.

The entire analyzer assembly was mounted in its

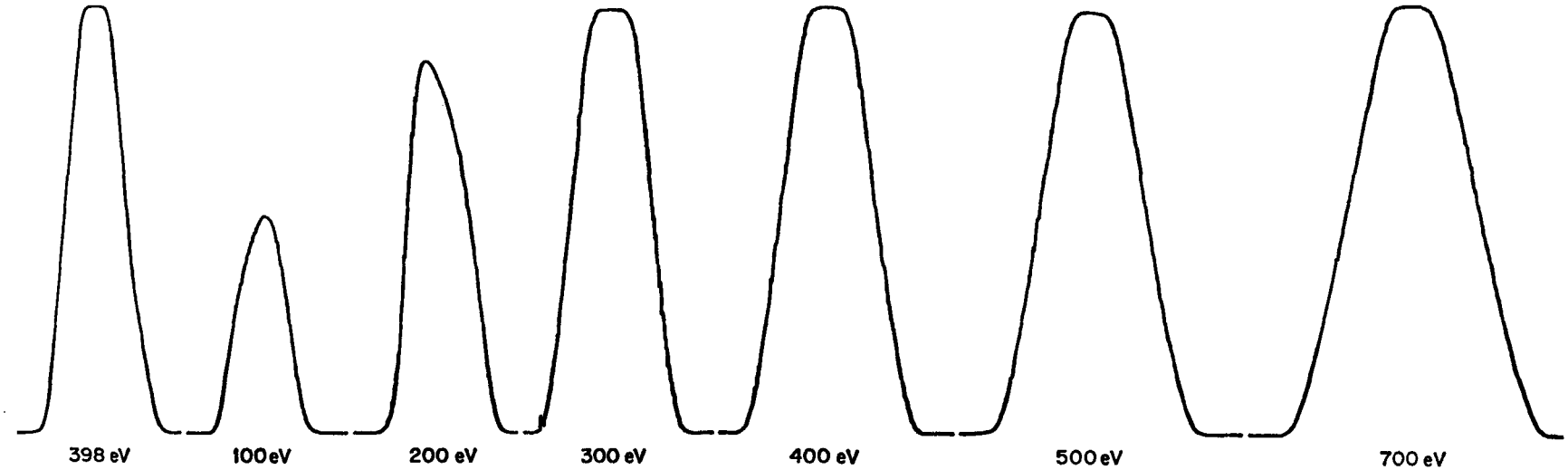

FIG. 5. Recorder traces of a 500-eV direct beam at various energies of analysis; I_0 was constant for all traces. The abscissa measures the voltage difference between inner and outer hemispheres; the ordinate, current passing through the analyzer. The flat maxima and constant peak heights for the higher analysis energies indicate that the transmission of the analyzer is 100%.

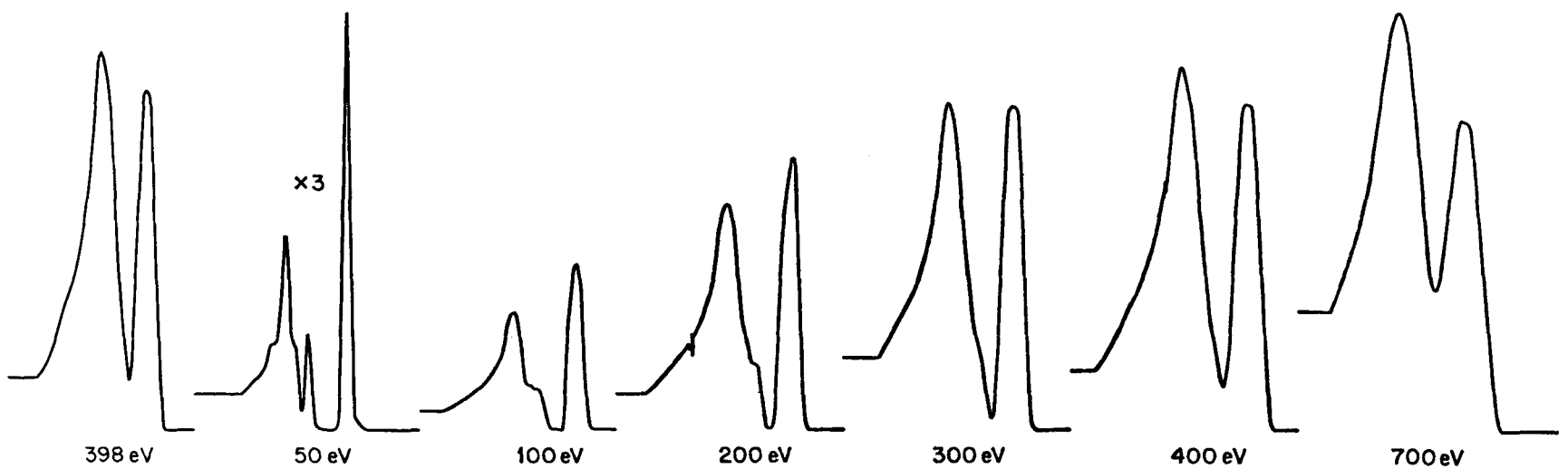

FIG. 6. CO spectra at a scattering angle of 2° at various energies of analysis indicating the resolution of the instrument. I_0 was a constant beam of 500-eV electrons. The elastic peaks are to the right. The separation between the elastic peak and the unresolved inelastic peak is about 10 eV.

housing (chamber III) and supported on a 4.25-in. bore thrust bearing (20). The center of mass of the assembly was moved toward the rotation axis by connecting a large, 16-lb counterweight (not shown) to the analyzer top plate (22). With the entire assembly mounted there was an almost imperceptible frictional resistance to rotation. Part (21) is a large, 6.00-in. pitch diameter, 60 teeth, 10 pitch, quadruple-thread stainless steel worm gear; the mating worm was aluminum. The worm is rotated through an NRC rotary harmonic feedthrough; one revolution of the feedthrough changes the scattering angle by $\frac{1}{3}°$. Angular settings could be reproduced to within 0.02°. Before each set of measurements the position of 0 angle was found by determining the positions of equal current on either side of the direct beam. A set of measurements was then made at a particular pressure by starting at a large positive angle, continuing through 0 and to large negative angles. Except for the largest angles, currents were measured at both $+\theta$ and $-\theta$ to average any errors due to misalignment, magnetic fields, or the position of the 0 angle. Agreement between positive and negative angles was quite good as seen in Fig. 8. The feedthrough was always turned in the same direction during any run. Following a run the position of the 0 angle was redetermined and usually found to be within 0.02° of the initial determination. I_0 was measured periodically during a run.

Pressure Measurement

Measurements were made at pressures between 0.1 and 2 mtorr for CO and N_2, and between 2 and 25 mtorr for He. When this research was started, it was felt that the only device capable of providing accurate, absolute pressure measurements in this region was the McLeod gauge.[6] The McLeod gauge suffers from a number of inherent disadvantages. It does not provide a continuous record of pressure, and the actual measurement itself is quite time consuming. The measurement is affected by unequal capillary effects in the tubes, and the use of a liquid nitrogen trap introduces large errors (as high as 20% have been reported by others) because of the streaming of mercury vapor as demonstrated by Ishii and Nakayama.[7]

The McLeod gauge was constructed in the glass shop at the Mellon Institute. The bulb volume was 398.1±0.5 ml; the average diameter of the capillary was 0.6756±0.0011 mm as measured by three different weighings of mercury slugs of length about 33 cm. The uniformity of the capillary bore was checked by measuring the length of a mercury slug at intervals of 5 cm along the 100-cm length of tubing. The average length of the slug was 6.358 cm; the average deviation at the 19 measured points was 0.033 cm. The capillary was cut so that the sealed end coincided with the most uniform region of the tube. The gauge constant was 9.005×10^{-7}.

TABLE II. Boyle's-law behavior in the McLeod gauge.

Height of Hg in side capillary above sealed end (mm)	h, Length of trapped gas column (mm)	h', Height of reference column above top of trapped column (mm)	Product hh' (mm²)
	$P\approx0.2$ (mtorr)		
+34	5.60	39.9	223
+46	4.54	50.3	228
+58	3.65	61.4	224
+78	2.73	80.5	220
+95	2.28	96.5	220
	$P\approx0.6$ (mtorr)		
+39	12.6	51.3	646
+57	9.75	66.5	648
+75	7.8	82.3	642

If we call h the length of trapped gas in the closed capillary, and h' the difference between reference and closed column heights, then the pressure is given by $9.005\times10^{-7}hh'$ torr, where h and h' are measured in millimeters. The gauge was used in the region where Boyle's law was valid, as determined by the constancy of the product hh' as both were varied. The characteristics of the gauge were such that unequal capillary forces introduced large deviations from Boyle's law if the height of the reference column was less than 30 mm above the sealed end, the product hh' increasing as the height of the mercury column was raised; above 30 mm Boyle's law was obeyed, the product hh' remaining constant as the column was raised. This behavior was confirmed for N_2 over a number of pressures from 0.1 to 1 mtorr. Two typical runs showing the constancy of hh' are summarized in Table II. All pressure measurements were made by opening the reservoir to atmospheric pressure, which raised the height of the column to about 55–60 mm above the sealed end.[8]

[6] It is our intention to add a capacitance manometer to our pressure measuring system, as it appears that their reliability has been improved in the millitorr region to the point where they may successfully replace McLeod gauges. In a preliminary check of our McLeod gauge against an MKS capacitance manometer acquired after the completion of these experiments, the pressures measured by the two gauges agreed to within 1% for He over the range 0.4–68 mtorr.

[7] H. Ishii and K. Nakayama, *Transactions of Eighth Vacuum Symposium and Second International Congress* (Pergamon Press, Inc., New York, 1961), Vol. 1, p. 519.

[8] By making h' greater than 60 mm, a capillary depression error as large as 1 mm will cause an error of only 1.7% in the pressure. By choosing suitably sensitive cathetometers, the errors in height measurements can be made quite small. It should be noted here that at the conclusion of our measurements we found one of our cathetometers to be subject to a reproducible error of 0.7% as used in reading the mercury meniscuses. We would recommend that catheometer users check their instruments against accurate scales. Our cross-section values have been corrected for this error.

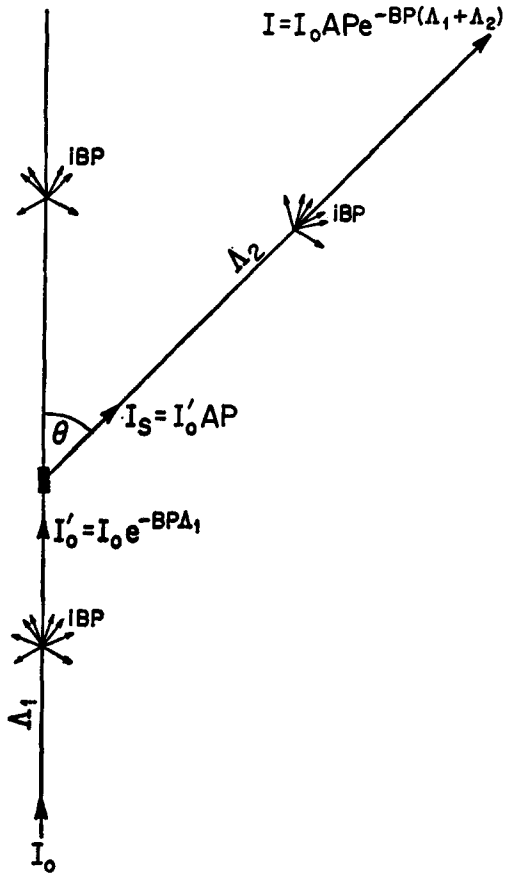

FIG. 7. Electron beam path through the scattering chamber showing attenuation of the beam.

The streaming error is caused by diffusion of Hg vapor from the gauge reservoir at room temperature to the liquid-N_2 trap. The only practical way to eliminate the error would be to operate the entire system, or just the gauge, under refrigeration at 0°C or lower, where the vapor pressure of Hg is negligibly small and introduces no significant error. It was felt that the cure was worse than the disease. Rather than eliminating the error, we measured it, and applied the measured correction to the pressure readings.

The entire system was pumped to below 10^{-8} torr, the vacuum pump shut off, and a small amount of gas admitted to the system. After equilibration the pressure, $P_{23°}$, was measured with the gauge. The mercury was then lowered to below the bulb cutoff, and the reservoir cooled to 0°C by immersion in an ice bath. After about 2 h of cooling, the gas in the bulb was trapped by raising the mercury above the cutoff. The ice bath was removed; the system was allowed to reach thermal equilibrium at room temperature, and the pressure $P_{0°}$ was then measured. The streaming error correction was taken as $P_{0°}/P_{23°}$. Three different determinations of the correction were made; N_2 at 1 and 0.5 mtorr, and CO at 0.25 mtorr; the corrections so determined were 1.056, 1.069, and 1.066, respectively. N_2 and CO are expected to have the same correction factors as their diffusion coefficients are almost the same. The correction for N_2 and CO was taken as 1.065. The correction for He was calculated to be 1.017 using the relationships given by Ishii and Nakayama, the experimental correction for N_2, and the diffusion coefficients for the respective gases. The pressures as determined by the gauge were multiplied by the proper correction factor.

A number of factors contribute uncertainties to the determination of the correction factor. Among these we may list: absorption and desorption of gases from walls and ceramic materials; partial cooling of the gas in the gauge bulb during cooling of the mercury reservoir; and the existence of tiny droplets of mercury along the walls of the gauge at room temperature while the bulk mercury is at 0°C. It is difficult to quantitatively assess these errors. The systematic error in pressure caused by the streaming error as a fraction of the pressure will be taken as 0.025 for N_2 and CO, and 0.01 for He, the smaller uncertainty for He reflecting the smaller value of the correction factor.

During a run pressures were measured at intervals of 1 h and were linearly interpolated with respect to time. Random errors in pressure measurements are incorporated in the errors as determined by the least-squared fitting process. The laboratory air conditioner was quite efficient in maintaining an ambient temperature of 23°C within limits of ±1.5°.

The Experimental Model

The expression for the absolute cross section, Eq. (1) contains the term I/I_0P. At constant pressure it has been verified that the ratio I/I_0 is independent of I_0 over a range of I_0 from 0.1 to 3 μA. On the other hand, the ratio I/I_0P is strongly dependent upon pressure. In order to operate in the region where the ratio is independent of pressure, P must be so low that either P or I, or both, cannot be measured with any accuracy. Thus measurements were made in the nonlinear pressure region and extrapolated to $P=0$.

The experimental model is shown in Fig. 7. Electrons enter the scattering chamber through the gun chamber exit pinhole (10) in the form of a narrow pencil of 1-mm diam with intensity I_0. Along the path electrons are continually scattered out of the beam because of both elastic and inelastic processes. This scattering, shown by the light arrows, varies as iBP, where P is the pressure, B is a constant related to the total scattering cross section (elastic plus inelastic) through the apparatus parameters, and i is the beam intensity along the path. Thus the final scattered intensity measured by the detector is

$$I=I_0AP\exp(-BP\Lambda), \qquad (4)$$

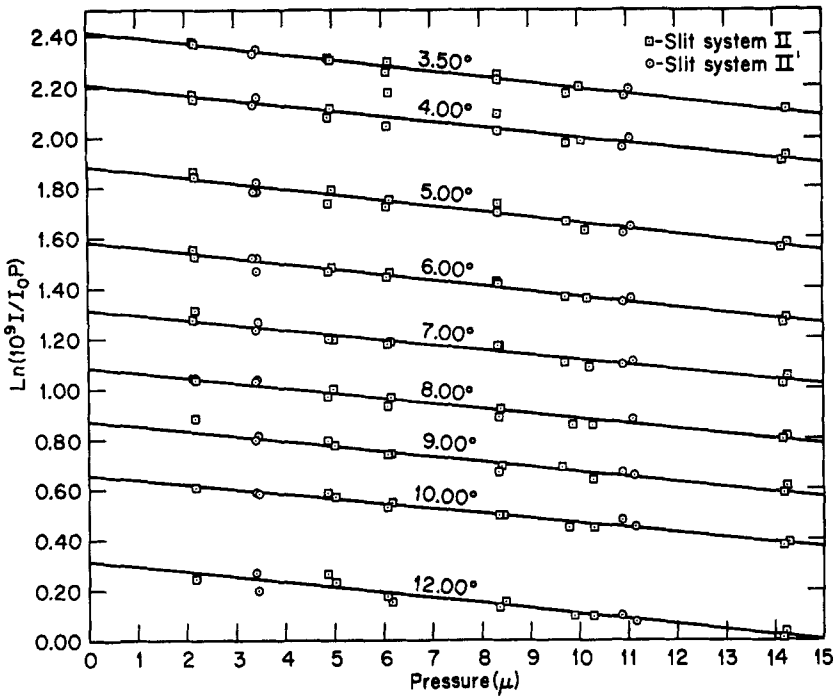

FIG. 8. Plots of $\ln(I/I_0P)$ vs P at different angles for He. The solid lines are the least-squares fitted lines. Points normally occur in pairs corresponding to measurements at positive and negative angles. Slit systems II and II' differ only in the size of the exit pinhole from the analyzer. That the circles and squares fall on the same straight line indicates that the transmission of the analyzer is 100%.

where $\Lambda=\Lambda_1+\Lambda_2$ is the total pathlength of an electron through the collision chamber. Equation (4) may be rearranged to give

$$\ln(I/I_0P)=\ln A-BP\Lambda. \qquad (5)$$

The primary beam detector is located 1–2 mm ahead of the exit pinhole, and thus measures I_0 directly. Plots of $\ln(I/I_0P)$ vs P should yield straight lines with slope $-B\Lambda$ and intercept $\ln A$. The ratio I/I_0P at zero pressure is thus determined by A; B provides a value for the total scattering cross section.

For each angle scattering currents were measured at at least five different pressures over a tenfold range of pressure, and Eq. (5) fitted to the data by the method of weighted least squares. The calculation provided values of A and the slopes together with their standard deviations. Figure 8 shows a set of such data points for He using slit system II; the solid lines are the least-squares fitted lines. Points were weighted according to the magnitudes of the pressures, currents, and agreement between measurements at positive and negative angles. In Fig. 8 points usually occur in pairs, corresponding to measurements at $+\theta$ and $-\theta$. The standard deviation for A was of the order of $0.01A$ or less for angles less than 20°, rising at higher angles; the fractional standard deviation in the slopes was of the order of 0.05.

It should be noted that the model does not take into account the possibility of electrons scattered out of the beam being rescattered into the beam, nor does it allow for different values of Λ for different electrons depending on the length of the scattering volume. Both factors would effect mainly the slopes of Eq. (5), retaining the general exponential form. Also the effects are expected to be largest at small angles. We observe that the slopes appear to decrease monotonically to about 20°, after which they appear to remain constant, as seen in Fig. 11. The χ^2 test of the goodness of fit applied to Eq. (4) indicates that the relationship is valid to a probability level greater than 0.995.

Data

Differential Elastic Cross Sections

Three different slit systems were used for N_2; measurements on CO and He were made with two different slit systems. The absolute elastic cross sections for N_2 are listed in Table III for each set of measurements. The slit geometry was such that at fixed angle and pressure the scattered currents from systems I, II, and III should be in the ratio of 1.0:2.6:17.4. The uncertainties reflect the fractional standard deviations in A as calculated by the computer in the least-squared fits. These uncertainties are a measure only of the random errors in the measurements within each slit system. The agreement between the values for different slit systems is a measure of the accuracy of our determinations of the slit dimensions.

Between 2° and 14° the absolute N_2 cross sections as measured by slit systems I, II, and III are in the ratio of 1.034:1.000:0.995 averaged over the angular range. (The 2° point for system III was here omitted). For the other two gases, the measurements for systems II and III are in the ratio of 1.000:0.982 and 1.000 to

TABLE III. Relative elastic cross sections normalized to $\sigma(\theta)=10.000$ at 10° for each gas.

	N_2	CO	He
2	44.82±0.46	46.58±0.34	25.92±0.18
2.5	40.73±0.24	42.41±0.42	23.27±0.11
3	37.22±0.25	38.95±0.21	21.80±0.07
3.5	34.22±0.16	35.85±0.21	20.14±0.09
4	31.53±0.31	32.51±0.18	18.78±0.11
5	26.31±0.10	27.14±0.19	16.69±0.20
6	22.15±0.08	22.65±0.12	14.98±0.08
7	18.27±0.08	18.65±0.11	13.42±0.07
8	15.08±0.07	15.29±0.10	12.15±0.05
9	12.26±0.07	12.36±0.07	11.01±0.06
10	10.000±0.057	10.000±0.057	10.000±0.079
12	6.522±0.036	6.455±0.059	8.386±0.036
14	4.212±0.028	4.178±0.028	7.020±0.062
16	2.805±0.031	2.797±0.028	5.883±0.036
18	1.956±0.017	1.948±0.016	4.772±0.039
20	1.435±0.014	1.462±0.012	3.950±0.011
25	0.909±0.011	0.963±0.010	2.466±0.012
30	0.656±0.011	0.674±0.007	1.600±0.016
35	0.459±0.007	0.448±0.010	1.037±0.006
40	0.290±0.007	0.288±0.007	0.709±0.011
45	0.195±0.005	0.191±0.005	0.493±0.007
50	0.135±0.005	0.136±0.004	0.356±0.006
55	0.109±0.003	0.115±0.005	0.258±0.007
60	0.094±0.004	0.098±0.005	0.193±0.005
65	0.080±0.003	0.084±0.002	

1.001 for CO and He, respectively. We stopped at 14° in this averaging process as the uncertainties for system I exceeded 1% at higher angles because of the smaller scattered currents. The results for the different slit systems agree to within the uncertainty in slit dimension measurements.

For each gas a set of cross sections was constructed by normalizing each set to the slit system III determinations, and then taking the weighted average of all available values at each angle. This set of normalized cross sections was then corrected to an "averaged" pinhole-slit dimension by multiplication by the factor 1.0049, which is the weighted average of the ratios of the individual slit system values to the normalized set values. Above 14°, only slit system III measurements were used, these likewise being corrected to the "averaged" dimension by the factor 1.0049.

Table IV lists relative cross sections for N_2, CO, and He normalized to $\sigma=10.000$ at 10° for each gas. Between 2° and 14° more than one value was available and the uncertainties are the usual variances obtained in weighted least-squared averaging. In a small number of cases the average deviation was larger than the variance, and was then used for the uncertainty. Above 14° only values for system III were used, and the uncertainties were obtained from the least-squares fitting calculation of Eq. (5).

Table V lists our best estimates of the absolute elastic collision cross sections for 500-eV electrons scattered from N_2, CO, and He. The calculated values of Khare and Moiseiwitsch[9] for He have been included in Table V for comparison. A separate column lists $(\Delta P)^2$ for each angle where ΔP is the momentum change in atomic units.

The uncertainties, δ, which appear after the ± symbols in Table V, expressed as factional uncertainties, are computed from the formula

$$\delta_{\text{fract}}^2=\delta_{\text{rand}}^2+\delta_P^2+\delta_I^2+\delta_{\text{slit}}^2+\delta_T^2+\delta_{\text{bg}}^2, \quad (6)$$

where δ_{rand} is the fractional uncertainty due to random errors in pressure measurements and current measurements, and are equal to the uncertainties in relative measurements; δ_P is the fractional systematic error in pressure measurements, taken as 0.025 for N_2 and CO, and 0.015 for He; δ_I is the fractional systematic error associated with current measurements, and is taken as 0.01 for all runs; δ_{slit} is the composite fractional

TABLE IV. Absolute elastic cross sections of N_2 at 500 eV from least-squares fits of Eq. (5) (units of a_0^2).

Angle	Slit system I	Slit system II	Slit system III
2°	76.00±0.46	72.74±0.41	79.48±1.42
2.5		66.68±0.41	66.69±1.10
3	63.32±0.39	60.59±0.33	61.33±0.83
3.5		56.12±0.29	55.47±0.58
4	54.14±0.37	51.23±0.28	51.11±0.49
5	44.40±0.34	43.17±0.22	42.78±0.35
6	37.73±0.28	36.20±0.20	35.99±0.22
7	30.74±0.30	29.96±0.16	29.82±0.29
8	25.61±0.19	24.68±0.16	24.47±0.22
9	20.53±0.27	20.11±0.13	20.04±0.22
10	16.84±0.23	16.44±0.11	16.17±0.20
12	10.94±0.14	10.70±0.08	10.64±0.13
14	7.05±0.11	6.92±0.07	6.89±0.08
16	4.62±0.08	4.60±0.06	4.57±0.05
18	3.08±0.08	2.97±0.06	3.18±0.03
20	2.77±0.28	2.36±0.06	2.34±0.02

[9] S. P. Khare and B. L. Moiseiwitsch, Proc. Phys. Soc. (London) 85, 821 (1965).

TABLE V. Best estimates of absolute elastic collision cross sections (in units of a_0^2).

Angle	N_2	CO	He	He[a] calculated	$(\Delta P)^2$
(0°)[b]	(104)	(109)	(1.89)	0.711	
2	73.40±2.50	76.23±2.54	1.4937±0.0478	0.691	0.0446
2.5	66.70±2.19	69.41±2.35	1.3409±0.0395	0.685	0.0695
3	60.96±2.02	63.75±2.09	1.2561±0.0356	0.677	0.1002
3.5	56.04±1.84	58.68±1.93	1.1609±0.0327	0.670	0.1368
4	51.63±1.75	53.21±1.75	1.0822±0.0307	0.661	0.1785
5	43.08±1.41	44.42±1.47	0.9617±0.0287	0.642	0.2787
6	36.27±1.18	37.08±1.22	0.8632±0.0241	0.620	0.4008
7	29.92±0.98	30.52±1.01	0.7734±0.0212	0.594	0.5449
8	24.69±0.81	25.02±0.83	0.6999±0.0190	0.567	0.7117
9	20.08±0.66	20.23±0.66	0.6344±0.0171	0.538	0.9004
10	16.37±0.54	16.37±0.54	0.5763±0.0158	0.507	1.1110
12	10.68±0.35	10.57±0.36	0.4833±0.0128	0.441	1.5982
14	6.90±0.22	6.83±0.22	0.4046±0.0110	0.380	2.1724
16	4.59±0.15	4.58±0.15	0.3390±0.0090	0.325	2.8336
18	3.20±0.11	3.19±0.11	0.2750±0.0074	0.276	3.5797
20	2.35±0.08	2.40±0.08	0.2277±0.0058	0.231	4.4113
25	1.488±0.051	1.576±0.053	0.1422±0.0037	0.148	6.8529
30	1.073±0.039	1.104±0.038	0.0922±0.0026	0.0928	9.7991
35	0.752±0.027	0.732±0.029	0.0598±0.0015	0.0610	13.2281
40	0.475±0.017	0.470±0.018	0.0409±0.0012	0.0429	17.1128
45	0.319±0.012	0.313±0.013	0.0284±0.0008	0.0290	21.4231
50	0.220±0.011	0.222±0.009	0.0205±0.0006	0.0208	26.1278
55	0.179±0.007	0.189±0.009	0.0149±0.0005	0.0151	31.1901
60	0.155±0.007	0.159±0.009	0.0111±0.0004	0.0113	36.5720
65	0.132±0.006	0.138±0.006			42.2319

[a] These values were obtained by drawing a smooth curve through the calculated values of Khare and Moiseiwitsch.[9] (The numbers, which do not appear in the paper, were kindly supplied by the authors.)

[b] Obtained by linear extrapolations of plots of $\ln\sigma$ vs θ for small angles. This extrapolation is not based on any particular model, and hence may be subject to large errors.

error due to slit and pinhole measurements and is taken as 0.01; δ_T is the fractional error due to temperature uncertainty, and is taken as 0.015 (see next section); δ_{bg} is the fractional error associated with the correction for background scattering currents. There was no background for CO or N_2. The background correction for He decreased monotonically from 4% at 1.5° to 0.4% at 25°. The fractional error in the background was taken as one-half the actual correction, and thus ranged from 0.02 at 1.5°, to 0.01 at 5°, and to 0.002 at 25°; it was taken as 0 at larger angles. The date of Table V are plotted in Figs. 9 and 10.

Temperature Correction

At the conclusion of the measurements we carefully rechecked each experimental parameter. We measured the temperature in the interior of the scattering chamber with suitably placed thermocouples, and found that the support for the primary beam Faraday cylinder (24) was 15°C above room temperature with the electron gun in operation. The support is about 1 cm from the beam path and extends along the entire length of the scattering volume; thus the true temperature of the scattering gas lies somewhere between 296° and

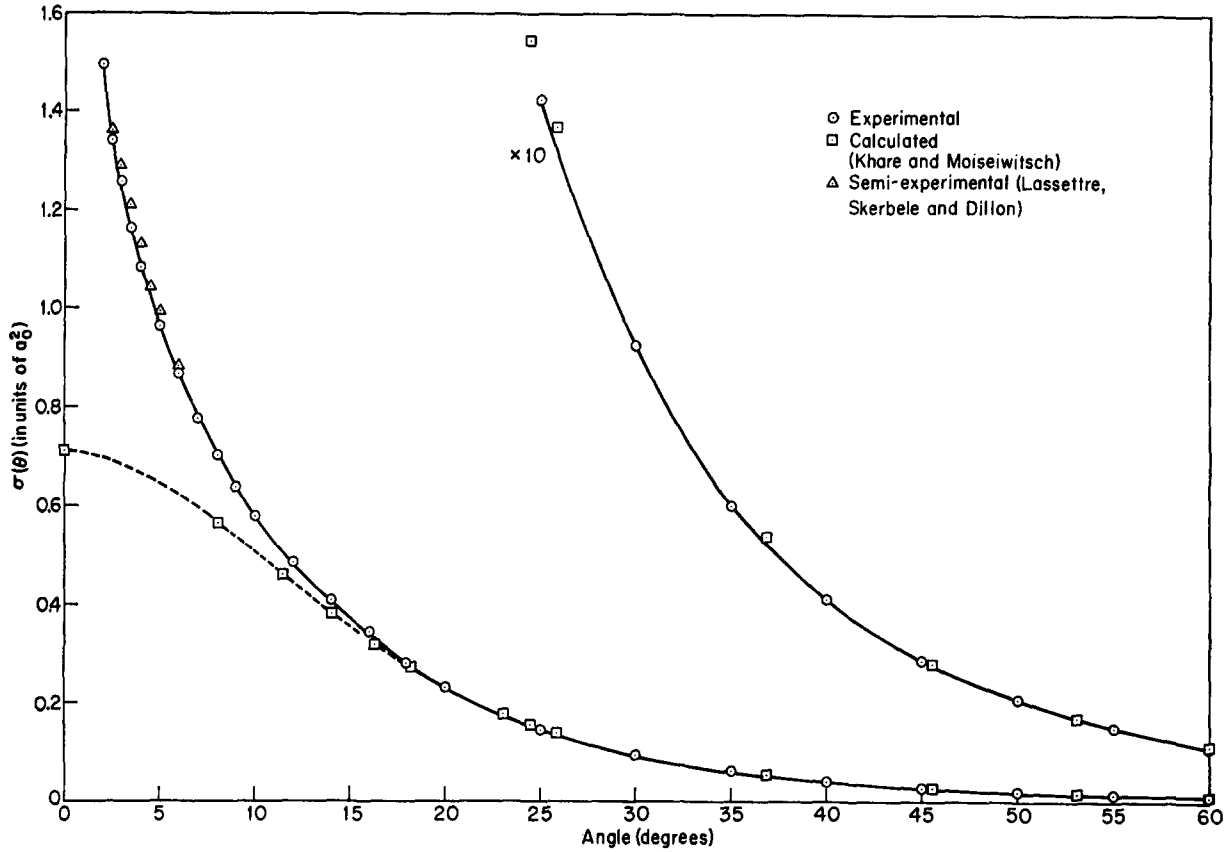

FIG. 9. Absolute elastic cross sections for 500-eV electrons scattered by He vs angle.

311°K. We have taken it to be 305°. This corresponds to a 3% deviation from room temperature. We estimate the uncertainty in this correction as one half the deviation or 1.5%.[10]

This temperature rise is due to heat conduction from the electron gun along the stainless steel tubing of the gun housing. We are presently constructing a new gun housing of copper in the hope of conducting this heat away from the scattering region.

Total Elastic Cross Sections

The total elastic cross sections were determined by graphical integration of curves of $\frac{1}{2}\sin\theta\sigma(\theta)$ vs θ. For He the calculated values of Khare and Moiseiwitsch were used for angles greater than 60°. For N_2 and CO at angles greater than 65° we simply scaled up the He values in that region. The error is probably small, as the contribution to the total elastic cross section because of scattering at angles larger than 65° is about 4% of the total scattering. Our values for σ_{tot} (elastic) in atomic units are 0.54, 0.57, and 0.027 for N_2, CO, and He, respectively.

The slopes of Eq. (5) are related to the total scattering cross section (elastic plus inelastic). The least-squares values of the slopes are plotted in Fig. 11. The slopes appear to decrease monotonically to about 16° after which there is no visible trend with angle. The total pathlength of an electron between the gun exit pinhole and the entrance pinhole to the analyzer is 19 cm. Half of this distance is between S-1 and S-2 where the pressure is equal to the pressure in the scattering chamber. In this region, electrons which have been doubly scattered through angles other than the angle of measurement may reach the entrance pinhole. This process greatly complicates the calculation of the total scattering cross section from the slopes, and no attempt has been made to do so. It is this process which causes the measured slopes to change so drastically with angle at small angles where the scattered currents are largest. This changing slope may vitiate

[10] A temperature rise of 15° corresponds to a 5% deviation from room temperature. In the limit of high pressure the correction to the gas density would be 5%; in the low-pressure limit, thermal transpiration would reduce the correction to the gas density to 2.5%. Except for the highest pressure runs on He, the mean-free paths of the gases were greater than 1 cm; thus we are operating near the free molecular flow region. The problem is further complicated by the fact that the gun housing and, especially, slit (10) are at a temperature greater than the cylinder support. Also the exact temperature is unknown as it is a function of the filament current and elapsed time. A temperature correction factor of 3%± 1.5% seems quite reasonable.

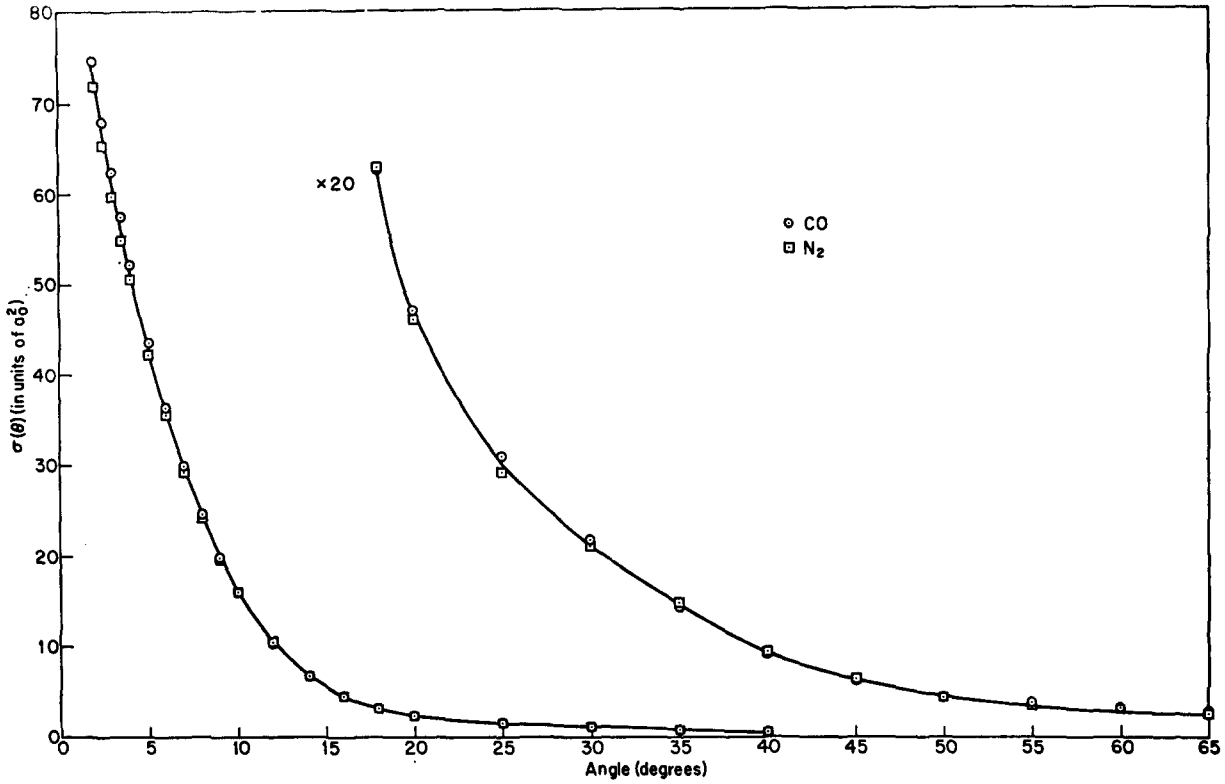

FIG. 10. Absolute elastic cross sections for 500-eV electrons scattered by N_2 and CO vs angle.

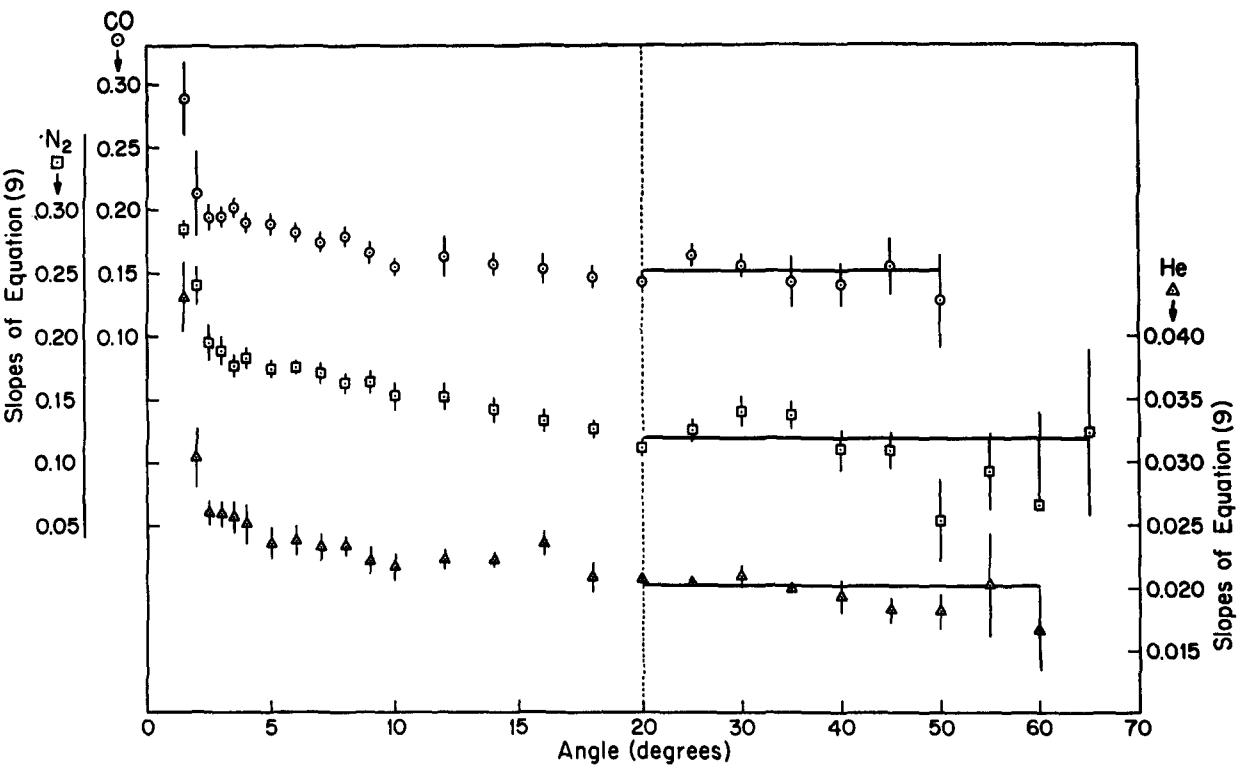

FIG. 11. Slopes of Eq. (5). The solid lines are the weighted means of all slopes at angles 20° and greater.

measurements of even relative cross sections at small angles unless the pressures are extremely low, or the measurements are extrapolated to zero pressure.

Discussion

Relative elastic cross sections of 500-eV electrons scattered by He have previously been measured by Hughes, McMillen, and Webb.[11] We have normalized their relative values to give exact agreement with our interpolated absolute cross section at 27°. The ratios of our interpolated values to the normalized values of Hughes *et al.* are then 1.226, 1.121, 0.980, 1.000, 0.838, 0.992, and 1.033 at 9.5°, 12°, 22°, 27°, 37°, 47°, and 57°, respectively.[12] It appears that the agreement is quite satisfactory at angles greater than 20°. (One might suspect that the large disagreement at 37° is due to a misprint in the original paper.) At small angles the previous results appear too low by 22% and 11% at 9.5° and 12°, respectively. It may well be that these discrepancies were caused by the inherent inaccuracies in working at their lower limit angles. Interestingly, these discrepancies were of the proper magnitude to provide agreement between calculated and measured cross sections. Elastic scattering cross sections for He have recently been calculated by Khare and Moiseiwitsch[9] based on the first Born approximation and first-order exchange approximation. Their calculated values are included in Fig. 9; Table V contains their values interpolated to angles at which measurements were made. Between 18° and 60° the calculated cross sections are consistently 2% higher than the experimental. The experimental uncertainties are of the order of 3%, thus the difference is not significant in this angular range. At smaller angles, however, the Born approximation calculation fails utterly, the experimental curve rising much more steeply than the theoretical; at 2° the experimental value is twice the theoretical. The deviation at small angles may be attributable to the omission of polarization in the calculation, or to an inherent deficiency in the first Born approximation. One would expect the inclusion of the polarization effect to raise the calculated values at small angles, which might provide a better fit to the data in this region. We now propose to extend our measurements to lower electron kinetic energies, which should provide a more critical test of the theoretical treatments.

Lassettre, Skerbele, and Dillon have recently determined absolute elastic cross sections for He in the range 2.5° to 6° in a semiexperimental manner.[13] They showed that the oscillator strength approaches the optical oscillator strength in the limit of zero momentum change; hence by extrapolation of experimental oscillator strengths from inelastic collisions they were able to place their inelastic cross sections on an absolute basis. Comparison of elastic and inelastic scattering currents then yielded absolute elastic cross sections. Their values so obtained are 1.36±0.04, 1.29±0.03, 1.21±0.03, 1.13±0.02, 0.99±0.04, and 0.88±0.03 at 2.5°, 3°, 3.5°, 4°, 5°, and 6°, respectively. Their measurements were done on a spectrometer of completely different mechanical and electron optical design. The excellent agreement in relative cross sections (better than 1%) enhances our confidence in the *shape* of the elastic scattering curve at small angles where inaccuracies in apparatus alignment and the spread in the primary beam may be important. Their absolute values are some 3% higher than ours, which is within the combined experimental uncertainties of the two measurements. It should be noted that the major portion of our uncertainty at angles below 45° arises from systematic errors, thus all the cross sections would deviate from the "true" cross sections in the same direction and by the same fractional amount if we are indeed experiencing a deviation at the outer limit of our uncertainty.

The absolute cross sections for N_2 and CO have been tabulated in Table V and plotted in Fig. 10. The two gases are isoelectronic. Thus, to a first approximation one would expect their elastic scattering behavior to be quite similar; this is precisely what we observe. At angles greater than 10° there is no significant difference between the measured cross sections for N_2 and CO. Below 10° the cross sections for CO increase at a slightly faster rate with decreasing angle than those for N_2. The differences are probably significant in this region, within confidence limits of about 90% (bearing in mind that the uncertainties indicated in Table V are absolute, and that the relative uncertainties are less.) The difference may be attributable to differences in polarization between the homonuclear and heteronuclear molecule.

ACKNOWLEDGMENTS

The author wishes to express his sincere thanks to E. N. Lassettre for suggesting this problem, and for many helpful discussions during the course of this work. The efforts of the Mellon Institute Machine Shop, and of A. Schubert, in particular, during the construction phase of this work is also gratefully acknowledged. We also thank C. E. Kuyatt for correcting some errors in our original calculation.

APPENDIX: CALIBRATION OF VIBRATING-REED ELECTROMETER

The scattered currents from the Faraday cylinder passed to ground through precision high resistances built into the electrometer. Currents were determined by measuring the voltage drop across the resistances. Our instrument contained four resistors, 10^8, 10^{10}, 10^{11},

[11] A. L. Hughes, J. H. McMillen, and G. M. Webb, Phys. Rev. **41**, 154 (1932).

[12] The normalization factor is 4.123×10^{16}; using this we obtain absolute cross sections from Hughes' data of 0.00655, 0.00470, 0.00253, 0.00230, 0.00180, 0.00118, and 0.00062 at 67°, 77°, 87°, 107°, 127°, 137°, and 147°, respectively.

[13] E. N. Lassettre, A. Skerbele, and M. A. Dillon, J. Chem. Phys. **49**, 2382 (1968).

and 10^{12} Ω; any of the four resistors could be switched into the circuit in a matter of seconds. Full scale output of the instrument could be varied from 0.001 to 30 V in 10 steps. By suitably choosing the pressure, incident beam current, and scattering angle, scattering currents were obtained which could be conveniently measured with at least two different resistors. This procedure enabled us to check the internal consistancy of the four resistors. We found the resistances to be in the ratio of $0.990\times10^{8}:0.986\times10^{10}:0.997\times10^{11}:1.000\times10^{12}$.

The maximum current measurable with the electrometer is 3×10^{-7} A. By adjusting the primary beam to slightly below this level I_0 could be measured with the electrometer using the 10^{8}-Ω resistor, and also with the microvolt amplifier by measuring the voltage drop across precision 1, 2, and 5 kΩ resistors. The current measured by the microvolt amplifier was larger by a factor of 1.030, yielding a value of 0.970×10^{8} Ω for the lowest electrometer resistor. The highest resistance, which was used exclusively for scattered currents, thus has a resistance of 0.980×10^{12} Ω.

The long-term stability of the resistance was checked against a commercial constant current source consisting of a small radium charged ionization chamber. The laboratory was air conditioned, and the resistances were found to be stable to better than 0.5% over a period of two years. This current source was also used to check the internal consistancy of the resistors, and the values obtained are included in the above ratios. In fact, for a short period of time we had access to three different constant current sources, and the internal consistancy was checked on all three. The manufacturer provided absolute calibrations of the current sources claimed to be good to 1%. Using the manufacturer's stated currents for the three sources we obtained values for the 10^{12}-Ω resistor of 0.983, 0.986, and 1.032×10^{12} Ω. The spread of some 5% necessitated our independent check.

THE JOURNAL OF CHEMICAL PHYSICS VOLUME 50, NUMBER 9 1 MAY 1969

Uniform Bounding Functions for a Certain One-Dimensional Form of Poisson's Equation

JOHN M. BOWNDS
Department of Mathematics, The University of Arizona, Tucson, Arizona
(Received 12 September 1968)

A classical one-dimensional specialization of the more general Poisson–Boltzman equation for potential space distributions associated with the existence of a double layer at an electrode surface leads to a certain nonlinear two-point boundary value problem. The classical approach to solving this problem involves a formal procedure which assumes a certain preknowledge of the actual unknown solution, and it involves finding an approximate solution which is obtained by deleting "higher-order" terms in a certain expansion. This paper presents a different approach in that it makes use of a known existence and uniqueness theorem to establish bounds on the actual solution to the problem. In certain examples, as shown in the paper, the actual effect of ignoring the so called higher-order terms in the classical approach can be clearly established.

I. INTRODUCTION

The following boundary value problem arises as a special case of the more general Poisson–Boltzman equation in the study of potential differences associated with the existence of a double layer at an electrode surface Ref. 1 and page 390 of Ref. 2,

$$\phi''(x)+\frac{4\pi e_0}{\epsilon}\sum_{i=1}^{n} z_i N_i \exp\left(-\frac{[z_i e_0\phi(x)]}{(kT)}\right)=0,$$

$$\phi(0)=\phi_0>0, \qquad \phi(+\infty)=0. \tag{1}$$

Here the quantities e_0, ϵ, k, T are assumed constant and have their usual significance. N_i and z_i represent the number of ions and the valence, respectively, of the ith ionic specie. n is the total number of species available to the electrochemical reaction.

The solution to (1) is difficult to obtain in its full generality, however, it is perhaps true that for some applications one is more interested merely in the "behavior" of the solution on the interval $0\leq x<+\infty$ rather than the actual solution itself. The purpose of this article is to make available a result due to Bailey, Shampine, and Waltman[3] which, as will be seen below, allows one to establish explicitly two exponentially decreasing functions $u_1(x)$ and $u_2(x)$ which have the property that if $\phi(x)$ is the solution to (1), then

$$u_1(x)\leq\phi(x)\leq u_2(x),$$

for $0\leq x<+\infty$. The sharpness of these bounding functions will, of course, be seen to depend upon the parameters appearing in (1). The existence of such functions u_1, u_2 will be proved below only for specific reactions for which the following equation holds:

$$\sum_{i=1}^{n} z_i N_i=0.$$

[1] P. Debye and E. Hückel, Physik Z. **24**, 185 (1923).
[2] G. Kortüm, *Treatise on Electrochemistry* (Elsevier Publ. Co., Inc., New York, 1965).
[3] P. Bailey, L. Shampine, and P. Waltman, J. Math. Anal. Appl. **14**, 433 (1966).